

Nonlinear Landau levels in the almost-bosonic anyon gas

Alireza Ataci,¹ Ask Ellingsen,¹ Filippa Getzner,¹ Théotime Girardot,² Douglas Lundholm,¹ and Dinh-Thi Nguyen^{3,4}

¹*Department of Mathematics, Uppsala University, Box 480, SE-751 06, Uppsala, Sweden*

²*Gran Sasso Science Institute, GSSI, 67100, L’Aquila, Italy*

³*Faculty of Mathematics and Computer Science, University of Science, Ho Chi Minh City, Vietnam*

⁴*Vietnam National University, Ho Chi Minh City, Vietnam*

We consider the quantitative description of a many-particle gas of interacting abelian anyons in the plane, confined in a trapping potential. If the anyons are modeled as bosons with a magnetic flux attachment, and if the total magnetic flux is small compared to the number of particles, then an average-field description becomes appropriate for the low-energy collective state of the gas. Namely, by means of a Hartree–Jastrow ansatz, we derive a two-parameter Chern–Simons–Schrödinger energy functional which extends the well-known Gross–Pitaevskii / nonlinear Schrödinger density functional theory to the magnetic (anyonic) self-interaction. One parameter determines the total number of self-generated magnetic flux units in the system, and the other the effective strength of spin-orbit self-interaction. This latter interaction can be either attractive/focusing or repulsive/defocusing, and depends both on the intrinsic spin-orbit interaction and the relative length scale of the flux profile of the anyons. Densities and energies of ground and excited states are studied analytically and numerically for a wide range of the parameters and align well with a sequence of exact nonlinear Landau levels describing Jackiw–Pi self-dual solitons. With increasing flux, counter-rotating vortices are formed, enhancing the stability of the gas against collapse. Apart from clarifying the relations between various different anyon models that have appeared in the literature, our analysis sheds considerable new light on the many-anyon spectral problem, and also exemplifies a novel supersymmetry-breaking phenomenon.

PACS numbers: 05.30.Pr, 03.75.Lm, 71.15.Mb, 73.43.-f

Keywords: quantum statistics, anyons, density functional theory, Thomas–Fermi approximation

Planar physics offers exciting possibilities by opening up for intermediate quantum statistics and anyons [1–7], with potentially groundbreaking applications in topological quantum information and computation [8–10]. However, despite recent advances in the experimental realization of individual anyons [11–14], a major obstacle to large-scale study of anyon physics is our yet limited theoretical understanding of the basic properties of the anyon gas; cf., e.g., the essential role of Gross–Pitaevskii (GP) theory for the study of Bose–Einstein condensation [15–17]. Namely, the key to unraveling the fundamental relationship between exchange and exclusion statistics for anyons is their enigmatic N -body spectral problem [18–20]. While $N = 2$ is analytically tractable, exhibiting a simple interpolation between the properties (energy, density, etc.) of bosons and fermions [1, 5, 6], only a small fraction of the spectrum is known analytically for $N \geq 3$ [21–23] and the remaining part has been investigated using numerical methods for small systems [24–27]. In the early 1990s, the qualitative behavior of the ideal N -anyon spectrum in a harmonic trap was studied [28, 29]. It showed a highly nontrivial interpolation in terms of angular momentum, and included some quantitative approximations close to bosons and fermions by means of density functionals. Around the same time, it was realized that pointlike but singular (point-interacting) anyons can exist [30–35], and may manifest a “noninterpolating” spectrum [22, 36]. A possible physical interpretation was given in terms of spin-orbit coupling and Pauli super-

symmetry [31, 37–39]. Anyon superconductivity was proposed for certain fractions of the statistics parameter relative to fermions [40–43], and a Chern–Simons theory of statistics transmutation developed in the context of the fractional quantum Hall effect (FQHE) [44–46], which in a certain self-dual limit admits exact vortex soliton solutions [47–54]. For a recent encyclopedic overview of known properties of the 2D anyon gas, see [55].

In recent times, precise mathematical methods have been developed to investigate the stationary N -body ground state [56–58] and to derive effective functional theories of Chern–Simons–Schrödinger (CSS) and Thomas–Fermi (TF) type [59–64]. In this Letter, we summarize some recent mathematical findings of physical importance for the abelian and almost-bosonic, interacting N -anyon problem [65, 66]. They include the derivation of an effective CSS model with precise relations for the physical parameters, its stability and supersymmetric properties, as well as the analysis of its emergent spectrum, numerically and analytically studied with the help of Jackiw–Pi vortex solitons or “nonlinear Landau levels” (NLLs).

Microscopic anyon Hamiltonian. For a microscopic description of the anyon gas, we consider the R -extended, N -anyon Hamiltonian, with α flux units per particle, and with spin-orbit coupling parameter g :

$$H_N := \sum_{j=1}^N \left[(-i\nabla_{\mathbf{x}_j} + \alpha \mathbf{A}_j^R)^2 + \frac{g}{2} \alpha B_j^R + V(\mathbf{x}_j) \right], \quad (1)$$

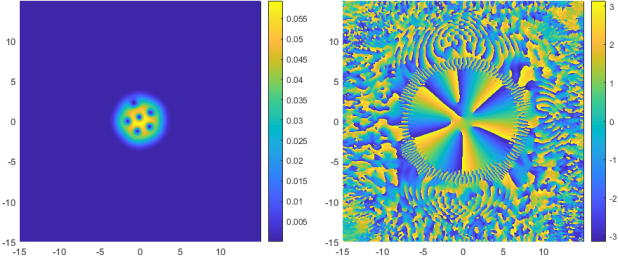


FIG. 1. Density and phase of an approximate minimizer for $E(\beta = 10, \gamma = 20\pi, V_h) \approx 9.066$.

where $\mathbf{x}_j \in \mathbb{R}^2$ is the position of the j :th particle, \mathbf{A}_j^R a planar vector potential in Coulomb gauge with magnetic field $B_j^R := \text{curl } \mathbf{A}_j^R = 2R^{-2} \sum_{k \neq j} \mathbf{1}_{D(\mathbf{x}_k, R)}(\mathbf{x}_j)$ (disks of radius R with flux 2π at \mathbf{x}_k), and V is a regular one-body trapping potential, i.e. $V(\mathbf{x}) \rightarrow \infty$ as $\mathbf{x} \rightarrow \infty$. Here we will consider the harmonic trap $V_h(\mathbf{x}) := \frac{1}{2}m\omega^2|\mathbf{x}|^2$. We normalize units $\hbar = 2m = \frac{\omega}{2} = 1$, and allow pointlike anyons by taking $R \rightarrow 0$ and $\mathbf{1}_{D(\mathbf{x}_k, R)}/(\pi R^2) \rightarrow \delta_{\mathbf{x}_k}$, the Dirac measure. Note that, even in the pointlike case at fixed N , there are different anyon types specified by g , where $g = \pm 2$ defines “ideal anyons” (regular/hard) and “kreinylons” (singular/soft), respectively; see [55, 66] for review. The Hamiltonian (1) acts on symmetric wave functions $\Psi_N \in L_{\text{sym}}^2(\mathbb{R}^{2N})$ s.t. $\alpha = 0$ corresponds to ideal bosons and $\alpha = 1$, $R = 0$ to ideal spinless fermions.

Mesoscopic CSS average-field functional. If $N \gg 1$ while the total flux $\alpha N \simeq \beta$ is of order 1, then on intermediate length scales $R \ll \ell \ll \omega^{-1/2}$ the interacting anyon gas is well described by the following Chern–Simons–Schrödinger (CSS) energy functional:

$$\mathcal{E}_{\beta, \gamma, V}[\phi] := \int_{\mathbb{R}^2} \left[|(-i\nabla + \beta \mathbf{A}_\varrho)\phi|^2 + \gamma|\phi|^4 + V|\phi|^2 \right]. \quad (2)$$

Here γ is an effective coupling parameter, $B_\varrho = \text{curl } \mathbf{A}_\varrho = 2\pi\varrho$ is a self-consistently generated magnetic field with density distribution $\varrho = |\phi|^2$, and $\phi \in L^2(\mathbb{R}^2)$ a one-body collective state, the CSS wave function (see Fig. 1). We denote the ground-state energy of (2), i.e. its infimum over regular ϕ subject to the normalization constraint $\|\phi\| = 1$, by $E(\beta, \gamma, V)$. For $\beta = 0$, (2) reduces to the GP energy functional in zero magnetic field.

To approximate the low-energy stationary states of the anyon gas, we use a Hartree–Jastrow ansatz for (1):

$$\Psi_N := C_N \prod_{i < j} f_{R/\ell}(|\mathbf{x}_i - \mathbf{x}_j|/\ell) \prod_{k=1}^N \phi(\mathbf{x}_k), \quad (3)$$

where $C_N > 0$ is a normalization constant s.t. $\|\Psi_N\| = 1$, $\phi \in L^2(\mathbb{R}^2)$ a smooth variational one-body state, and

$$f_s(r) := \begin{cases} \frac{4s^\alpha}{2(1+s^{2\alpha})+g(1-s^{2\alpha})}, & \text{if } 0 \leq r \leq s, \\ \frac{(2+g)r^\alpha+(2-g)s^{2\alpha}r^{-\alpha}}{2(1+s^{2\alpha})+g(1-s^{2\alpha})}, & \text{if } s \leq r \leq 1, \\ 1, & \text{if } r \geq 1. \end{cases}$$

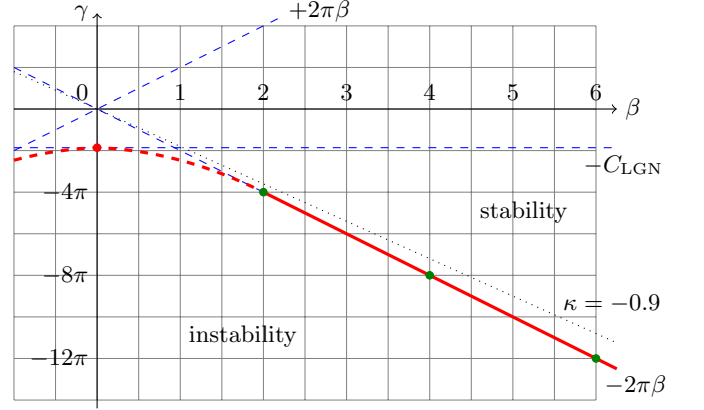


FIG. 2. Stability holds if and only if $E(\beta, \gamma, V) > -\infty$. NLLs exist at $\beta \in 2\mathbb{Z} \setminus \{0\}$ with the critical coupling $\gamma = -2\pi|\beta|$.

In [66] it is shown that, if $\alpha \simeq \beta/N$, $0 \leq R = \mathcal{O}(e^{-\sigma N}) \ll \ell = \mathcal{O}(N^{-\tau})$, and $\beta > 0$, $\sigma \geq 0$, $\tau > 2$, $g \geq 0$, then the energy per particle

$$\lim_{N \rightarrow \infty} N^{-1} \langle \Psi_N | H_N | \Psi_N \rangle = \mathcal{E}_{\beta, \gamma, V}[\phi], \quad (4)$$

where

$$\gamma = 2\pi\beta \frac{1 + \frac{g}{2} - (1 - \frac{g}{2})e^{-2\beta\sigma}}{1 + \frac{g}{2} + (1 - \frac{g}{2})e^{-2\beta\sigma}}. \quad (5)$$

Note that, in the “supersymmetric” case $g = \pm 2$ this yields exactly $\gamma = \pm 2\pi\beta$ for all relative scales $\sigma \sim N^{-1} \log \frac{\ell}{R}$. In the relatively dense limit $\sigma \rightarrow 0$ it becomes $\gamma = g\pi\beta$ whereas in the dilute limit $\sigma \rightarrow +\infty$, $g > -2$ it is $\gamma = 2\pi\beta$. We can also notice that in the non-interacting/“spinless” limit $g \rightarrow 0$ it is $\gamma = 2\pi\beta \tanh(\beta\sigma)$, and $\gamma = 2\pi\beta \coth(\beta\sigma)$ in the case of hard disks $g \rightarrow +\infty$, $\sigma > 0$. This extends the previously studied mean-field/Hartree case $\sigma = 0 = g$, $f_s = 1$, for which matching lower bounds are also available [59, 64, 67].

The derivation of the precise formula (5) was motivated by a previous result by Mashkevich [39] concerning the asymptotic 2-body energy. Namely, we define a relative s-wave “scattering energy” E_2 as the infimum of

$$\int_{D(0,1)} \left[|\nabla f|^2 + \alpha^2 \frac{|\mathbf{x}|^2}{\max\{R, |\mathbf{x}|\}^4} |f|^2 + \alpha g \frac{\mathbf{1}_{B(0,R)}}{R^2} |f|^2 \right],$$

with $f \in L^2$ regular on the unit disk with $f|_{r=1} = 1$. Then our function f_s captures this scattering energy to order α^2 , and its contribution to the N -body energy per particle as $N \rightarrow \infty$ (with $\binom{N}{2}$ pairs and relative mass 2) is $(N-1)E_2 \simeq \gamma$ as in (5); see [66]. Compare to the scattering length and energy for dilute Bose gases [68, 69], and note that the anyonic vector interaction is long ranged but suppressed by small α , while the spin-orbit scalar interaction is relatively short ranged.

Stability and supersymmetry. For each β there is a critical attractive coupling γ for the CSS model beyond

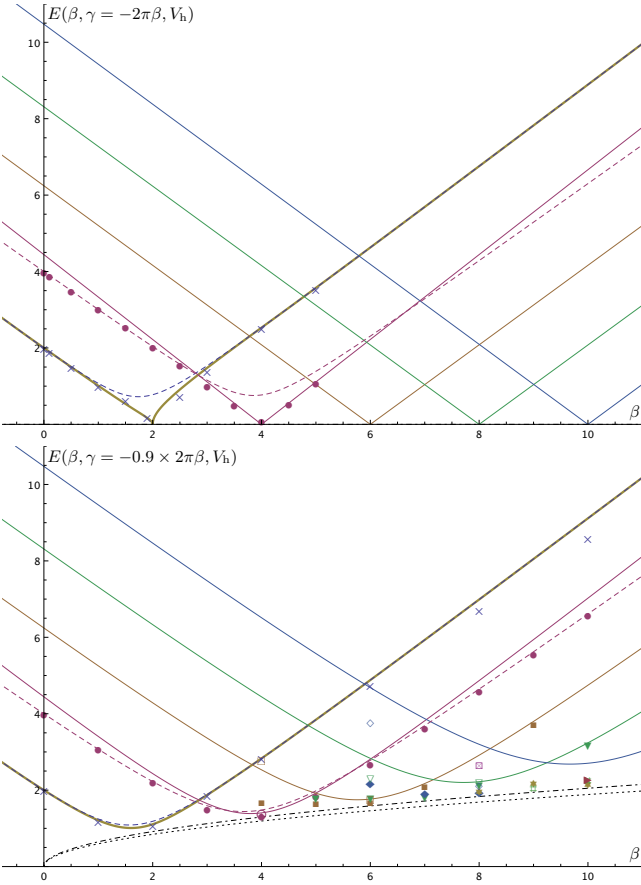


FIG. 3. Analytical and numerical energies for attractive gas $\gamma = 2\pi\beta\kappa < 0$ at $\kappa = -1$ (“kreinylons”) resp. $\kappa = -0.9$.

which the gas collapses; we denote it by $\gamma_*(\beta)$. Thus, for any (β, γ) s.t. $\gamma \geq -\gamma_*(\beta)$, we have $E(\beta, \gamma, V) > -\infty$ (stability), while if $\gamma < -\gamma_*(\beta)$ then $E(\beta, \gamma, V) = -\infty$ (instability); see Fig. 2. By scaling, it is sufficient to consider $V = 0$ and $E(\beta, \gamma, 0) = 0$ resp. $-\infty$, and the critical coupling $\gamma_*(\beta)$ is exactly the smallest (by infimum) ratio between the magnetic-kinetic self-energy $\mathcal{E}_{\beta,0,0}[\phi]$ and the scalar/electrostatic self-energy $\int |\phi|^4$ among all normalized and regular ϕ . Note the complex conjugation symmetry $\phi \rightarrow \bar{\phi}$, $\beta \rightarrow -\beta$, implying $\gamma_*(-\beta) = \gamma_*(\beta)$.

At $\beta = 0$, the critical attraction for stability of the GP functional is the constant $\gamma_*(0) =: C_{\text{LGN}} \approx 0.931 \times 2\pi$ (see [70]), realized by “Townes’ soliton” [71, 72], the real and unique solution (mod scaling and translation) at $E(0, -C_{\text{LGN}}, 0) = 0$. In [65] it was shown that $\gamma_*(\beta) = 2\pi\beta$ for $\beta \geq 2$, while for intermediate $0 < \beta < 2$ it holds that $\gamma_*(\beta) > \max\{C_{\text{LGN}}, 2\pi\beta\}$. Further, although as a limit $E(\beta, -2\pi\beta, 0) = 0$ for all $\beta \in \mathbb{R}$, zero-energy solutions only exist for $\beta = 2, 4, 6, \dots$, and we refer to these as “nonlinear Landau levels” (NLLs). Namely, at the self-dual coupling $\gamma = -2\pi\beta$, with $B = 2\pi\beta\varrho$,

$$\mathcal{E}_{\beta, -2\pi\beta, 0}[\phi] = \langle \phi | (-i\nabla + \mathbf{A})^2 - B | \phi \rangle. \quad (6)$$

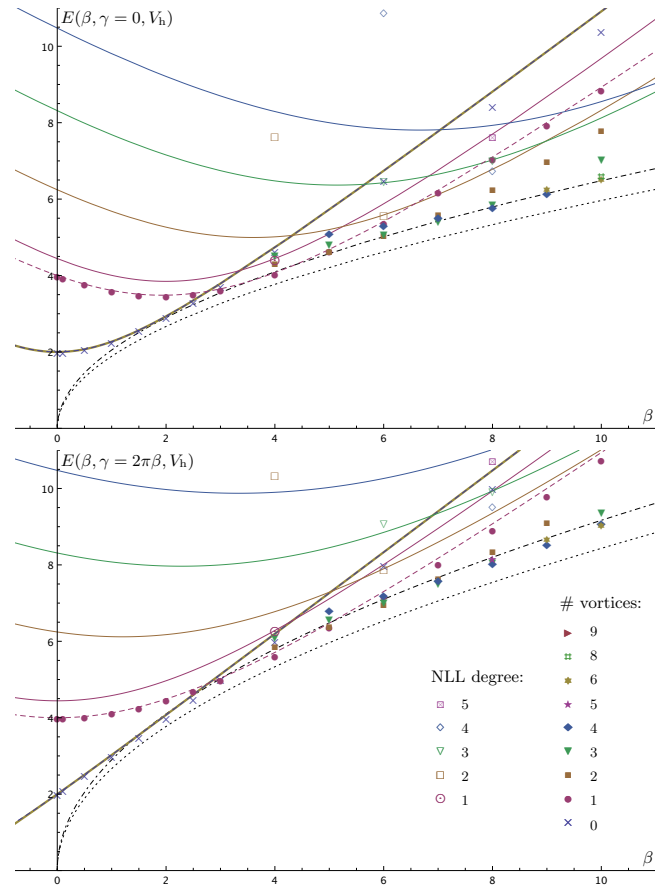


FIG. 4. Analytical and numerical energies for repulsive gas $\gamma = 2\pi\beta\kappa \geq 0$ at $\kappa = 0$ resp. 1 (ideal anyons). See the text.

If $\mathbf{A} = \frac{1}{2}(\partial_2, -\partial_1)\psi$, where the superpotential ψ solves $-\Delta\psi = 2B$, we can use the supersymmetric factorization

$$\mathcal{E}_{\beta, -2\pi\beta, 0}[\phi] = \int_{\mathbb{R}^2} |(\partial_1 - i\partial_2)(e^{-\psi/2}\phi)|^2 e^\psi. \quad (7)$$

Cf. the standard, *linear* Landau problem, where $B > 0$ is a constant and where the zero-energy subspace, the *lowest* Landau level, consists of all normalizable functions on the form $\phi = \overline{f(z)}e^{\psi/2}$, where f is analytic in $z = x_1 + ix_2 \in \mathbb{C}$, and $\psi(\mathbf{x}) = -B|\mathbf{x}|^2$. In our problem, ψ in (7) solves the nonlinear and nonlocal, generalized Liouville equation $-\Delta\psi = 4\pi\beta|f|^2e^\psi$, yielding the exact solutions [65]

$$f \propto P'Q - PQ', \quad \phi_{P,Q} := \sqrt{\frac{2}{\pi\beta}} \frac{\overline{P'Q - PQ'}}{|P|^2 + |Q|^2}, \quad (8)$$

where P, Q are linearly independent and coprime complex polynomials with $n := \max(\deg P, \deg Q) = \beta/2$. This complete set of regular minimizers includes all the self-dual soliton solutions found by Jackiw and Pi: initially, radial vortex rings with $P = z^n$ and $Q = 1$ [48], and eventually, the more general rationals P/Q [49]. Thus, along the critical line $\gamma = -2\pi\beta$, $\beta \in \mathbb{R}$, the sequence of points

$\beta = 2n$ mark a phase transition from strictly positive (broken supersymmetry) to zero energy and increasing degree of supersymmetry, exhibited by NLL manifolds of real dimension $4n$; compare Figs. 2 and 3 (top).

Macroscopic energy and density in a harmonic trap: numerics. For $\beta \gg 1$ and $\gamma \propto \beta$ in the stable regime, to minimize the energy we anticipate the formation of a locally homogeneous vortex lattice on scales $\ell \sim \beta^{-1/4}$; cf. [60–62]. In contrast to Abrikosov lattices in strong external magnetic fields [73, 74], the lattice spacing here follows the density profile sharply. Therefore, by local density approximation on the macroscopic scale of the trap, we expect an approximate Thomas–Fermi (TF) description to hold for a coarse-grained average density $\tilde{\varrho}$:

$$\mathcal{E}_{\beta, \gamma, V}[\phi] \approx \mathcal{E}_{G, V}^{\text{TF}}[\tilde{\varrho}] := \int_{\mathbb{R}^2} [G\tilde{\varrho}^2 + V\tilde{\varrho}], \quad (9)$$

subject to $\int \tilde{\varrho} = 1$, $V = V_h$, and a constant G depending on both β and γ . The minimum energy $E(\beta, \gamma, V_h) \simeq E^{\text{TF}}(G) = \frac{4}{3}\sqrt{G/\pi}$ and the minimizer $\varrho \approx \tilde{\varrho}^{\text{TF}} = (2G)^{-1}(\lambda^{\text{TF}} - |\mathbf{x}|^2)_+$. For comparison, $G = 2\pi N$ yields the asymptotic density and energy per particle of N spinless fermions in the harmonic trap.

In Figs. 3–4 we study the energy spectrum of (2) along the line $\gamma = 2\pi\beta\kappa$, for $\beta \in [0, 10]$ and four different slopes κ . When $\beta = \gamma = 0$ it is simply the Schrödinger energy of the 2D harmonic oscillator, with spectrum $2, 4, 6, \dots$. As upper bounds we have computed the analytical energies of the first few radial vortex rings ($n = 2, 3, 4, 5$; optimally rescaled) and of an approximation to the “versiera” at $n = 1$ with finite potential energy; these are the solid curves in the plots; see Supplementary Material (SM) for details. We have compared to the ground (Gaussian, at $n = 1$) and first excited (single counter-rotating vortex, at $n = 2$) states of the harmonic oscillator (again optimally rescaled; dashed curves). Further, general energies have been computed numerically (solid markers) by means of a gradient descent method, which is an extension of that used in [62] to the scalar self-interaction, with (β, γ) in the stable regime. We have tested its accuracy with $\beta = 0$ and various γ to reproduce GP energies; cf. [16, Table 3.5]. Also, at $\gamma = 0$ we reproduce the minimal energies of [62], i.e. the minima follow closely the estimate $E^{\text{TF}}(2\pi c\beta)$ where the numerical fit $c = 2\sqrt{\pi}/3 \approx 1.18$ is a renormalizing “Abrikosov factor” originating from the small-scale variations of the emerging vortex lattice. Interestingly, this behavior holds also for small β all the way down to $\beta \gtrsim 2$. The critical β for nucleation of a single vortex is just slightly below 3.

For a general estimate of the ground-state energy at $\gamma = 2\pi\beta\kappa$, $\kappa \geq -1$, we have compared with the linear interpolation $E^{\text{TF}}(2\pi c(1 + \kappa)\beta) = E^{\text{TF}}(2\pi\beta)\sqrt{c}\sqrt{1 + \kappa}$ (dash-dotted curve), which provides a fit to numerics to within a few percent for $\beta \gtrsim 3$ and $-0.9 \lesssim \kappa \lesssim 2$. The

estimate given by [28] for $\kappa = 1$ is ca 6% smaller. An absolute lower bound for the energy (assuming regularity and singlevaluedness) is provided by $\gamma_*(\beta) \rightarrow 2\pi\beta$ and thus differs by a factor \sqrt{c} , i.e. 9% (dotted curve; which for ideal anyons is still 41% higher than the ideal Fermi energy). We also conjecture that the real-valued minimizer at $\kappa = \pm 1$ has a linearly interpolating energy $|2\pm\beta|$. This, as well as other linear features of the $\kappa = \pm 1$ spectra, resembles the known linear/noninterpolating exact states of the N -anyon spectrum [22, 28, 36, 66].

For $\beta = 2n \in \{4, 6, 8\}$ we have used analytical expressions for the NLLs (from solving the inverse Wronskian problem $P, Q \mapsto W(P, Q) := P'Q - PQ'$) and numerical integration together with optimization of the placement of zeros/vortices to estimate their minimal energy

$$\mathcal{E}_{\beta, \gamma, V_h}[\phi_{P, Q}] = \int_{\mathbb{R}^2} [(4\pi n + \gamma)|\phi_{P, Q}|^4 + V_h|\phi_{P, Q}|^2]. \quad (10)$$

These are the hollow markers in the plots (again, see SM for details). Although for small β it is very costly to break the radial symmetry, there is a trend that for larger β and smaller γ this cost can be reduced in sufficiently symmetric vortex configurations, and indeed for $\beta = 8$, $\kappa = -0.9$ an NLL state with 4 separated vortices has lower energy than any of the radial vortex rings.

Conclusions and outlooks. We have derived and analyzed an effective CSS model of the interacting many-anyon gas in the bosonic limit, which manifests a spectrum of energies/states that are well describable using a family of exact NLLs (8). Although we have here focused on small flux $\beta \lesssim 10$, the Matlab part of our numerics extends to ca $\beta \lesssim 140$ (see Table XII in SM). Our study of exact NLLs is mainly limited by the increasing complexity of the inverse Wronskian problem, however we may extend relatively easily to some symmetry-reduced cases for $\beta \geq 10$. Ongoing work also includes external magnetic fields and the Abrikosov problem for self-generated vortex lattices. Further, in our analysis of NLLs we have assumed regularity and singlevaluedness of CSS wave functions ϕ . We believe that in order to obtain even lower energies, to eventually match the ideal Fermi energy at $\alpha \rightarrow 1$, we must relax these assumptions. This also leads to the study of systems of CSS functions and Liouville–Toda-type equations (cf. [75–77]), which will be addressed in future work. Some new insight into the fermionic side of the problem, via fermionic Hartree and magnetic TF theory, has been recently discussed in [78] (see also [79]).

In conclusion, we believe that important keys to understanding the complex interpolation between the almost-bosonic and almost-fermionic anyon spectra will come via the NLLs and their possible extension to more general functions. Also, exploring the two-parameter energy landscape may uncover fruitful and highly nontrivial relations between the CSS, GP, TF, and other models.

Acknowledgments. We are grateful to Romain Duboscq for the original Matlab code upon which much of our numerical work is based. A.A., A.E., F.G. and D.L. thank the Department of Mathematics of Politecnico di Milano for its kind hospitality during the spring of 2025 intensive period “Quantum Mathematics at Polimi”. D.L. also thanks the GSSI L’Aquila for its hospitality. All of us have benefited from discussions at the Institut Mittag-Leffler workshop “Anyons from small to large scales” in July 2025. Financial support from the Swedish Research Council (D.L., grant no. 2021-05328, “Mathematics of anyons and intermediate quantum statistics”) is gratefully acknowledged. A.A. thanks Kaj Nyström for the financial support for traveling to the relevant conferences. The author T.G. acknowledges the Gran Sasso Science Institute for the financial support making this work possible. A.E. gratefully thanks the Center for Interdisciplinary Mathematics at Uppsala University as well as C.F. Liljewalchs stipendiestiftelse for their financial support.

[1] J. M. Leinaas and J. Myrheim, *On the theory of identical particles*, Nuovo Cimento B **37** (1977), 1–23, [doi](#).

[2] G. Goldin, R. Menikoff, and D. Sharp, *Particle statistics from induced representations of a local current group*, J. Math. Phys. **21** (1980), no. 4, 650–664, [doi](#).

[3] G. A. Goldin, R. Menikoff, and D. H. Sharp, *Representations of a local current algebra in nonsimply connected space and the Aharonov-Bohm effect*, J. Math. Phys. **22** (1981), no. 8, 1664–1668, [doi](#).

[4] F. Wilczek, *Magnetic flux, angular momentum, and statistics*, Phys. Rev. Lett. **48** (1982), 1144–1146, [doi](#).

[5] F. Wilczek, *Quantum mechanics of fractional-spin particles*, Phys. Rev. Lett. **49** (1982), 957–959, [doi](#).

[6] Y.-S. Wu, *General theory for quantum statistics in two dimensions*, Phys. Rev. Lett. **52** (1984), 2103–2106, [doi](#).

[7] G. A. Goldin, R. Menikoff, and D. H. Sharp, *Comments on “General Theory for Quantum Statistics in Two Dimensions”*, Phys. Rev. Lett. **54** (1985), 603–603, [doi](#).

[8] A. Y. Kitaev, *Fault-tolerant quantum computation by anyons*, Ann. Physics **303** (2003), no. 1, 2–30, [doi](#).

[9] S. Lloyd, *Quantum computation with abelian anyons*, Quantum Inf. Process. **1** (2002), no. 1-2, 13–18, [doi](#).

[10] M. H. Freedman, A. Kitaev, M. J. Larsen, and Z. Wang, *Topological quantum computation*, Bull. Amer. Math. Soc. (N.S.) **40** (2003), no. 1, 31–38, Mathematical challenges of the 21st century (Los Angeles, CA, 2000), [doi](#).

[11] H. Bartolomei, M. Kumar, R. Bisognin, A. Marguerite, J.-M. Berroir, E. Bocquillon, B. Plaçais, A. Cavanna, Q. Dong, U. Gennser, Y. Jin, and G. Fève, *Fractional statistics in anyon collisions*, Science **368** (2020), no. 6487, 173–177, [doi](#).

[12] J. Nakamura, S. Liang, G. C. Gardner, and M. J. Manfra, *Direct observation of anyonic braiding statistics*, Nature Phys. **16** (2020), 931–936, [doi](#).

[13] Google Quantum AI and Collaborators, *Non-abelian braiding of graph vertices in a superconducting processor*, Nature **618** (2023), no. 7964, 264–269, [doi](#).

[14] N. Read and S. Das Sarma, *Clarification of braiding statistics in Fabry-Perot interferometry*, Nature Physics **20** (2024), 381–382, [doi](#).

[15] F. Dalfovo, S. Giorgini, L. P. Pitaevskii, and S. Stringari, *Theory of Bose-Einstein condensation in trapped gases*, Rev. Mod. Phys. **71** (1999), no. 3, 463–512, [doi](#).

[16] W. Bao and Y. Cai, *Mathematical theory and numerical methods for Bose-Einstein condensation*, Kinetic and Related Models **6** (2012), no. 1, 1–135, [doi](#).

[17] L. Pitaevskii and S. Stringari, *Bose-Einstein condensation and superfluidity*, vol. 164, Oxford University Press, 2016.

[18] G. S. Canright and S. M. Girvin, *Fractional statistics: quantum possibilities in two dimensions*, Science **247** (1990), no. 4947, 1197–1205, [doi](#).

[19] G. S. Canright and M. D. Johnson, *Fractional statistics: alpha to beta*, J. Phys. A: Math. Gen. **27** (1994), no. 11, 3579, [doi](#).

[20] A. Khare, *Fractional Statistics and Quantum Theory*, 2nd ed., World Scientific, Singapore, 2005.

[21] Y.-S. Wu, *Multiparticle quantum mechanics obeying fractional statistics*, Phys. Rev. Lett. **53** (1984), 111–114, [doi](#).

[22] C. Chou, *Multianyon spectra and wave functions*, Phys. Rev. D **44** (1991), 2533–2547, [doi](#).

[23] C. Chou, *Multi-anyon quantum mechanics and fractional statistics*, Phys. Lett. A **155** (1991), no. 4, 245–251, [doi](#).

[24] Y. Hatsugai, M. Kohmoto, and Y.-S. Wu, *Braid group and anyons on a cylinder*, Phys. Rev. B **43** (1991), 2661–2677, [doi](#).

[25] M. Sporre, J. J. M. Verbaarschot, and I. Zahed, *Numerical solution of the three-anyon problem*, Phys. Rev. Lett. **67** (1991), 1813–1816, [doi](#).

[26] M. V. N. Murthy, J. Law, M. Brack, and R. K. Bhaduri, *Quantum spectrum of three anyons in an oscillator potential*, Phys. Rev. Lett. **67** (1991), 1817–1820, [doi](#).

[27] M. Sporre, J. J. M. Verbaarschot, and I. Zahed, *Four anyons in a harmonic well*, Phys. Rev. B **46** (1992), 5738–5741, [doi](#).

[28] R. Chitra and D. Sen, *Ground state of many anyons in a harmonic potential*, Phys. Rev. B **46** (1992), 10923–10930, [doi](#).

[29] S. Li, R. K. Bhaduri, and M. V. N. Murthy, *Thomas-Fermi approximation for confined anyons*, Phys. Rev. B **46** (1992), 1228–1231, [doi](#).

[30] S. M. Girvin, A. H. MacDonald, M. P. A. Fisher, S.-J. Rey, and J. P. Sethna, *Exactly soluble model of fractional statistics*, Phys. Rev. Lett. **65** (1990), 1671–1674, [doi](#).

[31] J. Grundberg, T. Hansson, A. Karlhede, and J. Leinaas, *On singular anyon wavefunctions*, Mod. Phys. Lett. B **05** (1991), no. 07, 539–546, [doi](#).

[32] C. Manuel and R. Tarrach, *Contact interactions of anyons*, Phys. Lett. B **268** (1991), no. 2, 222–226, [doi](#).

[33] D. Sen and R. Chitra, *Anyons as perturbed bosons*, Phys. Rev. B **45** (1992), 881–894, [doi](#).

[34] M. Bourdeau and R. D. Sorkin, *When can identical particles collide?*, Phys. Rev. D **45** (1992), 687–696, [doi](#).

[35] S.-J. Kim and C. Lee, *Quantum description of anyons: Role of contact terms*, Phys. Rev. D **55** (1997), 2227–2239, [doi](#).

[36] M. V. N. Murthy, J. Law, R. K. Bhaduri, and G. Date, *On a class of noninterpolating solutions of the many-anyon problem*, J. Phys. A: Math. Gen. **25** (1992), no. 23,

6163, [doi](#).

[37] M. Y. Choi, C. Lee, and J. Lee, *Soluble many-body systems with flux-tube interactions in an arbitrary external magnetic field*, Phys. Rev. B **46** (1992), 1489–1497, [doi](#).

[38] A. Comtet, S. Mashkevich, and S. Ouvry, *Magnetic moment and perturbation theory with singular magnetic fields*, Phys. Rev. D **52** (1995), 2594–2597, [doi](#).

[39] S. Mashkevich, *Finite-size anyons and perturbation theory*, Phys. Rev. D **54** (1996), 6537–6543, [doi](#).

[40] R. B. Laughlin, *The Relationship between High-Temperature Superconductivity and the Fractional Quantum Hall Effect*, Science **242** (1988), 525–533, [doi](#).

[41] A. L. Fetter, C. B. Hanna, and R. B. Laughlin, *Random-phase approximation in the fractional-statistics gas*, Phys. Rev. B **39** (1989), 9679–9681, [doi](#).

[42] Y. H. Chen, F. Wilczek, E. Witten, and B. I. Halperin, *On anyon superconductivity*, Int. J. Mod. Phys. B **03** (1989), 1001–1067, [doi](#).

[43] F. Wilczek, *Fractional Statistics and Anyon Superconductivity*, World Scientific, Singapore, 1990.

[44] S. C. Zhang, T. H. Hansson, and S. Kivelson, *Effective-field-theory model for the fractional quantum Hall effect*, Phys. Rev. Lett. **62** (1989), 82–85, [doi](#).

[45] A. Lopez and E. Fradkin, *Fractional quantum Hall effect and Chern-Simons gauge theories*, Phys. Rev. B **44** (1991), 5246–5262, [doi](#).

[46] Z. Ezawa, M. Hotta, and A. Iwazaki, *Field theory of anyons and the fractional quantum Hall effect*, Physical Review B **46** (1992), no. 12, 7765.

[47] R. Jackiw and E. J. Weinberg, *Self-dual Chern-Simons vortices*, Phys. Rev. Lett. **64** (1990), 2234–2237, [doi](#).

[48] R. Jackiw and S.-Y. Pi, *Soliton solutions to the gauged nonlinear Schrödinger equation on the plane*, Phys. Rev. Lett. **64** (1990), 2969–2972, [doi](#).

[49] R. Jackiw and S.-Y. Pi, *Classical and quantal nonrelativistic Chern-Simons theory*, Phys. Rev. D **42** (1990), 3500–3513, [doi](#).

[50] C. R. Hagen, *Comment on “Soliton solutions to the gauged nonlinear Schrödinger equation on the plane”*, Phys. Rev. Lett. **66** (1991), 2681–2681, [doi](#).

[51] R. Jackiw and S.-Y. Pi, *Jackiw and Pi reply*, Phys. Rev. Lett. **66** (1991), 2682–2682, [doi](#).

[52] R. Jackiw, *Self-dual Chern—Simons solitons*, Mathematical Physics X (Berlin, Heidelberg) (K. Schmüdgen, ed.), Springer Berlin Heidelberg, 1992, pp. 184–212, [doi](#).

[53] G. V. Dunne, *Aspects of Chern-Simons theory*, Aspects topologiques de la physique en basse dimension. Topological aspects of low dimensional systems (Berlin, Heidelberg) (A. Comtet, T. Jolicœur, S. Ouvry, and F. David, eds.), Springer Berlin Heidelberg, 1999, pp. 177–263, [doi](#).

[54] P. A. Horvathy and P. Zhang, *Vortices in (abelian) Chern-Simons gauge theory*, Physics Reports **481** (2009), no. 5–6, 83–142, [doi](#).

[55] D. Lundholm, *Properties of 2D anyon gas*, Encyclopedia of Condensed Matter Physics (Second Edition) (T. Chakraborty, ed.), Academic Press, Oxford, 2nd ed., 2024, pp. 450–484, [arXiv:2303.09544](#), [doi](#).

[56] D. Lundholm and J. P. Solovej, *Local exclusion principle for identical particles obeying intermediate and fractional statistics*, Phys. Rev. A **88** (2013), 062106, [doi](#).

[57] D. Lundholm, *Many-anyon trial states*, Phys. Rev. A **96** (2017), 012116, [doi](#).

[58] D. Lundholm and V. Qvarfordt, *Exchange and exclusion in the non-abelian anyon gas*, arXiv e-prints, 2020, [arXiv:2009.12709](#).

[59] D. Lundholm and N. Rougerie, *The average field approximation for almost bosonic extended anyons*, J. Stat. Phys. **161** (2015), no. 5, 1236–1267, [doi](#).

[60] M. Correggi, D. Lundholm, and N. Rougerie, *Local density approximation for the almost-bosonic anyon gas*, Analysis & PDE **10** (2017), 1169–1200, [doi](#).

[61] M. Correggi, D. Lundholm, and N. Rougerie, *Local density approximation for almost-bosonic anyons*, Proceedings of QMath13, Atlanta, October 8–11, 2016, Mathematical problems in quantum physics (F. Bonetto, D. Borthwick, E. Harrell, and M. Loss, eds.), Contemp. Math., vol. 717, 2018, pp. 77–92, [doi](#).

[62] M. Correggi, R. Duboscq, D. Lundholm, and N. Rougerie, *Vortex patterns in the almost-bosonic anyon gas*, EPL (Europhysics Letters) **126** (2019), 20005, [doi](#).

[63] T. Girardot and N. Rougerie, *Semiclassical limit for almost fermionic anyons*, Commun. Math. Phys. **387** (2021), no. 1, 427–480, [doi](#).

[64] T. Girardot, *Mean-field approximation for the anyon gas*, Ph.D. thesis, Université Grenoble Alpes & CNRS, l’École Doctorale Mathématiques, Sciences et technologies de l’information, Informatique, 2021, <https://www.theses.fr/2021GRALM031>.

[65] A. Ataei, D. Lundholm, and D.-T. Nguyen, *A generalized Liouville equation and magnetic stability*, arXiv e-prints, 2024, [arXiv:2404.09332](#).

[66] A. Ataei, T. Girardot, and D. Lundholm, *Microscopic derivation of the stationary Chern-Simons-Schrödinger equation for almost-bosonic anyons*, arXiv e-prints, 2025, [arXiv:2504.17488](#).

[67] F. L. A. Visconti, *Average-field approximation for very dilute almost-bosonic anyon gases*, arXiv e-prints, 2025, [arXiv:2507.01102](#).

[68] E. H. Lieb, R. Seiringer, J. P. Solovej, and J. Yngvason, *The mathematics of the Bose gas and its condensation*, Oberwolfach Seminars, Birkhäuser, 2005, [arXiv:cond-mat/0610117](#).

[69] J. P. Solovej, *Mathematical physics of dilute Bose gases*, Comptes Rendus. Physique **26** (2025), 339–348 (en), [doi](#).

[70] M. I. Weinstein, *Nonlinear Schrödinger equations and sharp interpolation estimates*, Comm. Math. Phys. **87** (1983), 567–576, [doi](#).

[71] R. Y. Chiao, E. Garmire, and C. H. Townes, *Self-trapping of optical beams*, Phys. Rev. Lett. **13** (1964), 479–482, [doi](#).

[72] G. Fibich, *The nonlinear Schrödinger equation*, vol. 192, Springer, 2015.

[73] A. Aftalion, X. Blanc, and J. Dalibard, *Vortex patterns in a fast rotating Bose-Einstein condensate*, Phys. Rev. A **71** (2005), no. 2, 023611, [doi](#).

[74] A. Fetter, *Rotating trapped Bose-Einstein condensates*, Rev. Mod. Phys. **81** (2009), 647, [doi](#).

[75] G. V. Dunne, R. Jackiw, S.-Y. Pi, and C. A. Trugenberger, *Self-dual Chern-Simons solitons and two-dimensional nonlinear equations*, Phys. Rev. D **43** (1991), 1332–1345, [doi](#).

[76] G. Dunne, *Chern-Simons solitons, Toda theories and the chiral model*, Commun. Math. Phys. **150** (1992), no. 3, 519–535, [doi](#).

[77] C. Kim, C. Lee, P. Ko, B.-H. Lee, and H. Min, *Schrödinger fields on the plane with $[\mathrm{U}(1)]^N$ Chern-Simons interactions and generalized self-dual solitons*,

Phys. Rev. D **48** (1993), 1821–1840, [doi](#).

[78] A. Levitt, D. Lundholm, and N. Rougerie, *Magnetic Thomas-Fermi theory for 2D abelian anyons*, arXiv e-prints, 2025, [arXiv:2504.13481](#).

[79] Y. Hu, G. Murthy, S. Rao, and J. K. Jain, *Kohn-Sham density functional theory of abelian anyons*, Phys. Rev. B **103** (2021), 035124, [doi](#).

SUPPLEMENTARY MATERIAL

Here we give all the information necessary to reproduce the plots of Figs. 3–4. After setting our conventions, we first derive some explicit analytical NLL states (8) by solving the inverse Wronskian problem. Then we analytically compute the energies of some related trial states, including a reference Gaussian, the first excited harmonic oscillator energy eigenstates, powers of the “versiera” ansatz, as well as NLL “vortex rings”. Finally, we give tables of numerical data.

Notation and choice of gauge

The R -extended anyon gauge vector potential is defined by $\mathbf{A}_j^R := \sum_{k \neq j} \frac{(\mathbf{x}_j - \mathbf{x}_k)^\perp}{|\mathbf{x}_j - \mathbf{x}_k|^2_R}$ where $\mathbf{x}^\perp := (-x_2, x_1)$ denotes the counterclockwise 90° rotation for $\mathbf{x} = (x_1, x_2) \in \mathbb{R}^2$, and $|\mathbf{x}|_R := \max\{R, |\mathbf{x}|\}$. The effective gauge potential for a given density distribution $\varrho \in L^1(\mathbb{R}^2; \mathbb{R}_+)$ is defined by the convolution

$$\mathbf{A}_\varrho(\mathbf{x}) := \int_{\mathbb{R}^2} \frac{(\mathbf{x} - \mathbf{y})^\perp}{|\mathbf{x} - \mathbf{y}|^2} \varrho(\mathbf{y}) d\mathbf{y}.$$

In both vector potentials we have chosen the Coulomb gauge $\nabla \cdot \mathbf{A} = 0$, and they generate the magnetic fields

$$B_j^R = \operatorname{curl}_{\mathbf{x}_j} \mathbf{A}_j^R = \begin{cases} \frac{2}{R^2} \sum_{k \neq j} \mathbb{1}_{D(\mathbf{x}_k, R)}(\mathbf{x}_j), & R > 0, \\ 2\pi \sum_{k \neq j} \delta(\mathbf{x}_j - \mathbf{x}_k), & R = 0, \end{cases}$$

respectively

$$B_\varrho = \operatorname{curl} \mathbf{A}_\varrho = 2\pi \varrho$$

(in two dimensions, the magnetic field is a (pseudo-scalar quantity), where we used that $\Delta \log |\mathbf{x}| = 2\pi \delta(\mathbf{x})$. Throughout, we use the notation $D(\mathbf{x}, r)$ for a disk of radius r at \mathbf{x} , and $\mathbb{1}_\Omega$ for the characteristic function or projection operator supported on Ω . Also, $x_+ := \max\{0, x\}$. Sometimes we use complex notation for the coordinates $z = x_1 + ix_2 = re^{i\theta} \in \mathbb{C}$, $\bar{z} = x_1 - ix_2$.

Note that, because of our gauge choice and vanishing condition $\lim_{\mathbf{x} \rightarrow \infty} \mathbf{A}_\varrho = 0$, for a radially symmetric density $\varrho(\mathbf{x}) = \varrho(r)$, we must have

$$\mathbf{A}_\varrho(\mathbf{x}) = A(r) \mathbf{e}_\theta, \quad (11)$$

for some radial function $A(r)$. Stokes’ theorem then implies that

$$2\pi r A(r) = \oint_{\partial D(0, r)} \mathbf{A}_\varrho \cdot d\mathbf{s} = \int_{D(0, r)} \operatorname{curl} \mathbf{A}_\varrho = 2\pi \int_{D(0, r)} \varrho,$$

so

$$A(r) = \frac{1}{r} \int_{D(0, r)} \varrho = \frac{2\pi}{r} \int_0^r \varrho(s) s ds. \quad (12)$$

The Euler–Lagrange equation for a minimizing ground state or a stationary point ϕ of (2) is the CSS equation

$$[(-i\nabla + \beta \mathbf{A}_\varrho)^2 - 2\beta \nabla^\perp (\log |\cdot|) * \mathcal{J}_\phi + 2\gamma \varrho + V] \phi = \mu \phi, \quad (13)$$

where

$$\mathcal{J}_\phi := \frac{1}{2} \bar{\phi} (-i\nabla + \beta \mathbf{A}_\varrho) \phi + \text{h.c.}$$

and

$$\mu = 2\mathcal{E}_{\beta, \gamma, V}[\phi] - \int_{\mathbb{R}^2} \left[|\nabla \phi|^2 + V \varrho - \beta^2 |\mathbf{A}_\varrho|^2 \varrho \right]; \quad (14)$$

see [60, Appendix] and [65, Remark 3.11].

NLL states and inverse Wronskian problem

The general formula (8) for NLL states is parametrized by the space of solutions (P, Q) of the inverse Wronskian problem

$$W(P, Q) := P'Q - PQ' = f, \quad (15)$$

where f is a given polynomial and P and Q are coprime (and linearly independent) polynomials satisfying the degree condition $\max\{\deg P, \deg Q\} = n = \beta/2 > 0$.

Due to the determinantal property of the Wronskian and the symmetry of the amplitude $|P|^2 + |Q|^2$, the corresponding NLL state $\phi_{P, Q}$ given by (8) is invariant under pointwise action of the group $\text{SU}(2) \times \mathbb{R}^+$ on the space of polynomial pairs (P, Q) . It follows that we may without loss of generality assume that P or Q is monic, and, e.g., that $\deg Q < \deg P = n = \beta/2$. We may also simplify the problem (15) by adding any multiple of Q to P . If we identify states that differ only by multiplication by a constant phase factor $e^{i\theta}$, we have a further $\text{U}(1)$ -symmetry, for a full $\text{U}(2) \times \mathbb{R}^+$ -symmetry in total. See [65] for further details.

Thus, given the location of vortices/zeros $w_k \in \mathbb{C}$, i.e. $f(z) \propto \prod_k (z - w_k)$, we may enumerate all NLL solutions with these vortices by

$$(\tilde{P}, \tilde{Q}) = (P + \eta Q, \lambda^{-1} Q), \quad \eta \in \mathbb{C}, \quad \lambda > 0,$$

and

$$\phi_{\tilde{P}, \tilde{Q}} = \frac{1}{\sqrt{\pi n}} \frac{\overline{W(P, Q)}}{\lambda |P + \eta Q|^2 + \lambda^{-1} |Q|^2}, \quad (16)$$

where (P, Q) are particular solutions to the Wronskian problem (15) of the simplified form.

Notice that the number of vortices for a given NLL state $\phi_{P, Q}$ (counting multiplicities) is precisely $\deg W(P, Q)$, which for fixed $\beta/2 = n = \max\{\deg P, \deg Q\}$ is restricted by the inequalities

$$n - 1 \leq \deg W(P, Q) \leq 2n - 2. \quad (17)$$

Hence the n :th NLL space contains states with between $n - 1$ and $2n - 2$ vortices. We will now list some known NLL solutions for various n .

For any positive integer $n = \beta/2 = 1, 2, 3, \dots$, we may consider the degenerate case

$$f(z) = n(z - w)^{n-1}, \quad w \in \mathbb{C}.$$

A particular solution to the inverse Wronskian problem $W(P, Q) = f$ is then

$$P(z) = (z - w)^n, \quad Q(z) = 1. \quad (18)$$

The corresponding state on the form (16) is the “**vortex ring**”

$$\phi_{\tilde{P}, \tilde{Q}}(z) = \sqrt{\frac{n}{\pi}} \frac{(\bar{z} - \bar{w})^{n-1}}{\lambda |(z - w)^n + \eta|^2 + \lambda^{-1}}, \quad (19)$$

for $\lambda > 0$ and $\eta \in \mathbb{C}$. For $\eta = 0$, the corresponding density is radially symmetric about w . These solutions (for $w = \eta = 0$) were first described by Jackiw and Pi in [48]. For $n > 1$, they have a vortex (zero) of degree $n - 1$ at $z = w$, but in the special case $n = 1$, we get the real-valued and positive “**versiera**” solution

$$\phi(z) = \frac{1}{\sqrt{\pi}} \frac{1}{\lambda |z - w|^2 + \lambda^{-1}}, \quad (20)$$

which lacks vortices (note that the parameter η can be absorbed into w in this case). The family of versiera solutions, parametrized by the scale $\lambda > 0$, center $w \in \mathbb{C}$, and a constant phase, is the complete manifold of NLL states for $n = 1$.

For fixed $n = \beta/2$, the $4n$ -dimensional manifold of NLL states foliates over the degree $d = \deg f$, $n - 1 \leq d \leq 2(n - 1)$. For $n = 1$, we must have $d = 0$, so the versiera solutions are the only possible solutions. For $n = 2$ and $d = 1$, we have the particular solution

$$f(z) = z - w, \quad P(z) = z^2 - 2wz, \quad Q(z) = \frac{1}{2}, \quad (21)$$

corresponding to the family of vortex ring solutions (19) of degree 1, and for $d = 2$ we have the particular solution

$$\begin{aligned} f(z) &= (z - w_1)(z - w_2), \\ P(z) &= z^2 - w_1 w_2, \\ Q(z) &= z - \frac{w_1 + w_2}{2}. \end{aligned} \quad (22)$$

We must have $w_1 \neq w_2$, for otherwise P and Q are not coprime. Hence, these states have two separated vortices located at w_1 and w_2 . With the additional degrees of freedom in (16), these two families of solutions exhaust the NLL manifold for $n = 2$ (this was discussed in [65, Section 2.3]).

For $n = 3$, we have $2 \leq d \leq 4$ by (17). For $d = 2$, we have the particular solution

$$\begin{aligned} f(z) &= (z - w_1)(z - w_2), \\ P(z) &= z^3 - 3 \frac{w_1 + w_2}{2} z^2 + 3w_1 w_2 z, \quad Q(z) = \frac{1}{3}, \end{aligned} \quad (23)$$

with $w_1, w_2 \in \mathbb{C}$. If $w_1 = w_2$, this is a vortex ring of degree 2. For $d = 3$, we have two particular solutions:

$$\begin{aligned} f(z) &= (z - w_1)(z - w_2)(z - w_3), \\ P(z) &= z^3 - A_{\pm} z^2 + 2s_3, \\ Q(z) &= \frac{1}{2}z - \frac{1}{6}A_{\mp}, \end{aligned} \quad (24)$$

where

$$A_{\pm} := s_1 \pm \sqrt{s_1^2 - 3s_2}.$$

Here

$$s_k = s_k(w_1, \dots, w_d) := \sum_{1 \leq i_1 < \dots < i_k \leq d} w_{i_1} \cdots w_{i_k}$$

is the k :th elementary symmetric polynomial in the variables w_1, \dots, w_d . In particular,

$$\begin{aligned} s_1(w_1, w_2, w_3) &= w_1 + w_2 + w_3, \\ s_2(w_1, w_2, w_3) &= w_1 w_2 + w_1 w_3 + w_2 w_3, \\ s_3(w_1, w_2, w_3) &= w_1 w_2 w_3. \end{aligned}$$

For $d = 4$, we have the particular solutions

$$\begin{aligned} f(z) &= (z - w_1)(z - w_2)(z - w_3)(z - w_4), \\ P(z) &= z^3 - \frac{1}{2}B_{\mp} z + \frac{1}{2}s_3, \\ Q(z) &= z^2 - \frac{1}{2}s_1 z + \frac{1}{6}B_{\pm}, \end{aligned} \quad (25)$$

where

$$B_{\pm} := s_2 \pm \sqrt{s_2^2 - 3s_1 s_3 + 12s_4}.$$

These particular solutions yield all NLL states for $n = 3$ via (16).

For $n = 4$, we will be content with giving some special solutions with additional symmetries that have been used in the numerics. With $d = \deg f$ as usual, we have $3 \leq d \leq 6$. For $d = 3, 4$, we can for example place the vortices at a distance R from the origin along the roots of unity, $w_k = Re^{i2\pi k/d}$. This yields the particular solutions

$$f(z) = z^3 - R^3, \quad P(z) = z^4 - 4R^3 z, \quad Q(z) = \frac{1}{4}, \quad (26)$$

for $d = 3$, and

$$f(z) = z^4 - R^4, \quad P(z) = z^4 + 3R^4, \quad Q(z) = \frac{1}{3}z, \quad (27)$$

for $d = 4$. For $d = 5$, we may place one vortex at the origin and the other four along the roots of unity, yielding the particular solution

$$f(z) = z(z^4 - R^4), \quad P(z) = z^4 + R^4, \quad Q(z) = \frac{1}{2}z^2. \quad (28)$$

Analytical energies of trial states

We will now calculate the exact energy $\mathcal{E}[\phi] = \mathcal{E}_{\beta,\gamma,V}[\phi]$ analytically for certain trial CSS states ϕ in the harmonic trap $V(z) = V_h(z) = |z|^2$. The parameters β and γ are considered fixed.

First we make some general observations. By expanding the kinetic-magnetic term $|(\nabla + i\mathbf{A}_\varrho)\phi|^2$, the energy functional can be recast into the form

$$\mathcal{E}[\phi] = \int_{\mathbb{R}^2} [|\nabla\phi|^2 + 2\beta\mathbf{A}_\varrho \cdot \mathbf{J}_\phi + \beta^2|\mathbf{A}_\varrho|^2\varrho + \gamma\varrho^2 + V\varrho], \quad (29)$$

where

$$\mathbf{J}_\phi := \frac{i}{2}(\phi\nabla\bar{\phi} - \bar{\phi}\nabla\phi) \quad (30)$$

is the probability current induced by ϕ . When ϕ has a constant phase, $\mathbf{J}_\phi = 0$.

Now we turn to the question of finding the optimal length scale in the harmonic potential V_h , or equivalently the optimal scale of the trial state. If ϕ is a normalized trial state and $\lambda > 0$, let

$$\phi_\lambda(z) := \lambda\phi(\lambda z). \quad (31)$$

The rescaling $\phi \rightarrow \phi_\lambda$ induces rescalings of the quantities derived from ϕ :

$$\begin{aligned} \nabla\phi_\lambda(z) &= \lambda^2(\nabla\phi)(\lambda z); \\ \varrho_\lambda(z) &:= |\phi_\lambda(z)|^2 = \lambda^2\varrho(\lambda z); \\ \mathbf{A}_\lambda(z) &:= \mathbf{A}_{\varrho_\lambda}(z) = \lambda\mathbf{A}_\varrho(\lambda z); \\ \mathbf{J}_\lambda(z) &:= \mathbf{J}_{\phi_\lambda}(z) = \lambda^3\mathbf{J}_\phi(\lambda z). \end{aligned}$$

As a result, if we let

$$K_\lambda := \int_{\mathbb{R}^2} [|(\nabla + i\beta\mathbf{A}_\lambda)\phi_\lambda|^2 + \gamma\varrho_\lambda^2], \quad (32)$$

$$U_\lambda := \int_{\mathbb{R}^2} V_h\varrho_\lambda, \quad (33)$$

then $K_\lambda = \lambda^2 K_1$ and $U_\lambda = \lambda^{-2} U_1$, while $\int_{\mathbb{R}^2} \varrho_\lambda = 1$. Hence, the total energy is

$$E_\lambda := \mathcal{E}[\phi_\lambda] = K_\lambda + U_\lambda = \lambda^2 K_1 + \lambda^{-2} U_1, \quad (34)$$

which achieves its minimum at the optimal scaling parameter

$$\lambda_* := (U_1/K_1)^{1/4}. \quad (35)$$

Using (34), the corresponding minimal energy is

$$E_{\lambda_*} = 2\sqrt{K_1 U_1}. \quad (36)$$

Gaussian

We now compute the energy $\mathcal{E}[\phi] = \mathcal{E}_{\beta,\gamma,V_h}[\phi]$ analytically for some trial states ϕ , starting with a radially symmetric, Gaussian state

$$\phi(z) = \frac{1}{\sqrt{\pi}} e^{-r^2/2}, \quad (37)$$

where $r = |z|$. The corresponding density is

$$\varrho(z) = |\phi(z)|^2 = \frac{1}{\pi} e^{-r^2},$$

satisfying the normalization condition $\int_{\mathbb{R}^2} \varrho = 1$. Using (12), we get the corresponding magnetic potential

$$\mathbf{A}_\varrho(z) = \frac{2}{r} \left(\int_0^r s e^{-s^2} ds \right) \mathbf{e}_\theta = \frac{1}{r} (1 - e^{-r^2}) \mathbf{e}_\theta. \quad (38)$$

Since ϕ is real, $\mathbf{J}_\phi = 0$. The kinetic energy is

$$\int_{\mathbb{R}^2} |\nabla\phi|^2 = 2\pi \int_0^\infty \left| \frac{\partial\phi}{\partial r} \right|^2 r dr = 2 \int_0^\infty r^3 e^{-r^2} dr = 1,$$

where we used the standard integral

$$\int_0^\infty x^{2k+1} e^{-ax^2} dx = \frac{k!}{2a^{k+1}}, \quad k \in \mathbb{N}_0, a > 0. \quad (39)$$

The magnetic self-energy is given by

$$\int_{\mathbb{R}^2} |\mathbf{A}_\varrho|^2 \varrho = 2 \int_0^\infty \frac{(1 - e^{-r^2})^2 e^{-r^2}}{r} dr = \log \frac{4}{3},$$

which can be derived from the standard integral

$$\int_0^\infty \frac{e^{-ax} - e^{-bx}}{x} dx = \log \frac{b}{a}, \quad a, b > 0, \quad (40)$$

by expanding the integrand and substituting $t = r^2$. The scalar self-interaction energy is

$$\int_{\mathbb{R}^2} \varrho^2 = \frac{2}{\pi} \int_0^\infty r e^{-2r^2} dr = \frac{1}{2\pi},$$

and thus

$$K_1 = 1 + \beta^2 \log \frac{4}{3} + \frac{\gamma}{2\pi}.$$

Finally, the potential energy in the harmonic trap $V(z) = V_h(r) = r^2$ is

$$U_1 = \int_{\mathbb{R}^2} V_h \varrho = 2 \int_0^\infty r^3 e^{-r^2} dr = 1,$$

once again using (39).

Now consider ϕ_λ . At the optimal scaling parameter $\lambda = \lambda_*$ (see (36)), the total energy is

$$\mathcal{E}_{\beta,\gamma,V_h}[\phi_{\lambda_*}] = 2\sqrt{1 + \beta^2 \log \frac{4}{3} + \frac{\gamma}{2\pi}}. \quad (41)$$

With $\gamma = 2\pi\beta\kappa$, this is shown as the dashed blue curve in the plots.

Excited harmonic oscillator eigenstates

The Gaussian is the ground state of the harmonic oscillator. Now, we consider the two angular momentum eigenmodes of the first excited state:

$$\phi^+(z) = \frac{1}{\sqrt{\pi}}ze^{-|z|^2/2}, \quad \phi^-(z) = \frac{1}{\sqrt{\pi}}\bar{z}e^{-|z|^2/2}.$$

In polar coordinates $z = re^{i\theta}$, we have

$$\phi^\pm(z) = \frac{1}{\sqrt{\pi}}re^{-r^2/2}e^{\pm i\theta}.$$

The density is the same for both modes:

$$\varrho(z) = |\phi^\pm(z)|^2 = \frac{1}{\pi}r^2e^{-r^2},$$

and this is normalized to $\int_{\mathbb{R}^2} \varrho = 1$. Using (12), the corresponding magnetic potential is $\mathbf{A}_\varrho = A(r)\mathbf{e}_\theta$, with

$$A(r) = \frac{2}{r} \int_0^r s^3 e^{-s^2} ds = \frac{1 - (1 + r^2)e^{-r^2}}{r}.$$

Differentiating ϕ^\pm yields

$$\begin{aligned} \nabla \phi^\pm &= \frac{1}{\sqrt{\pi}}e^{\pm i\theta}e^{-r^2/2} [(1 - r^2)\mathbf{e}_r \pm i\mathbf{e}_\theta] \\ &= \frac{\phi_\pm}{r} [(1 - r^2)\mathbf{e}_r \pm i\mathbf{e}_\theta]. \end{aligned}$$

The currents for the two modes are therefore

$$\mathbf{J}_\pm := \mathbf{J}_{\phi^\pm} = \pm \frac{\varrho}{r} \mathbf{e}_\theta = \pm \frac{1}{\pi}re^{-r^2} \mathbf{e}_\theta.$$

The harmonic oscillator energy contributions are

$$\int_{\mathbb{R}^2} |\nabla \phi^\pm|^2 = \int_{\mathbb{R}^2} V_h \varrho = 2,$$

which can be verified either by direct computation using (39), or by using that ϕ^\pm are energy eigenstates of the harmonic oscillator. The scalar self-energy is given by

$$\int_{\mathbb{R}^2} \varrho^2 = \frac{2}{\pi} \int_0^\infty r^5 e^{-2r^2} dr = \frac{1}{4\pi}.$$

The magnetic self-energy common to both modes is given by

$$\int_{\mathbb{R}^2} |\mathbf{A}_\varrho|^2 \varrho = 2 \int_0^\infty r e^{-r^2} \left(1 - 2(1 + r^2)e^{-r^2}\right) dr = \frac{7}{54},$$

again using (39). The contribution due to the current is

$$\int_{\mathbb{R}^2} \mathbf{J}_\pm \cdot \mathbf{A}_\varrho = \pm 2 \int_0^\infty r e^{-r^2} \left(1 - (1 + r^2)e^{-r^2}\right) dr = \pm \frac{1}{4}.$$

The total energy is thus

$$K_1 = 2 + \frac{1}{4\pi}\gamma + \frac{7}{54}\beta^2 \pm \frac{1}{2}\beta, \quad U_1 = 2.$$

At the optimal scaling parameters $\lambda = \lambda_\pm$ (see (36)), we have the minimal energies

$$\mathcal{E}_{\beta, \gamma, V_h} [\phi_{\lambda_\pm}^\pm] = 2\sqrt{4 + \frac{\gamma}{2\pi} + \frac{7}{27}\beta^2 \pm \beta}. \quad (42)$$

Notice however that the optimal scales λ_\pm differ for the plus and minus modes ϕ^\pm . The negative mode (counter-rotating vortex) gives the lowest energy for $\beta > 0$ and is shown as the dashed purple curve in the plots.

Powers of the versiera

Another radially symmetric state is the “versiera” state (20) centered at the origin,

$$\phi(z) = \frac{1}{\sqrt{\pi}} \frac{1}{r^2 + 1}, \quad (43)$$

which is an NLL state at $\beta = 2$. It however has a divergent potential energy. More generally, we can take this state to a positive power $a \geq 1$ (and normalize), yielding the state

$$\phi^a(z) := \sqrt{\frac{2a-1}{\pi}} \frac{1}{(r^2 + 1)^a}. \quad (44)$$

The corresponding density is

$$\varrho^a(r) = \frac{2a-1}{\pi} \frac{1}{(r^2 + 1)^{2a}},$$

which satisfies $\int_{\mathbb{R}^2} \varrho^a = 1$. The corresponding magnetic potential is

$$A(r) = \frac{1}{r} \left(1 - \frac{1}{(r^2 + 1)^{2a-1}}\right).$$

Since ϕ^a is real, $\mathbf{J}_{\phi^a} = 0$.

The kinetic energy is

$$\int_{\mathbb{R}^2} |\nabla \phi^a|^2 = \int_{\mathbb{R}^2} \left| \frac{\partial \phi^a}{\partial r} \right|^2 = \frac{2a(2a-1)}{2a+1}.$$

The potential energy in a harmonic trap diverges logarithmically for $a = 1$, but for $a > 1$ we get a finite energy contribution

$$\int_{\mathbb{R}^2} V_h \varrho^a = (2a-1) \int_0^\infty \frac{r^2}{(1+r^2)^{2a}} \cdot 2r dr = \frac{1}{2(a-1)}.$$

The scalar self-energy is

$$\int_{\mathbb{R}^2} (\varrho^a)^2 = \frac{1}{\pi} \frac{(2a-1)^2}{4a-1}.$$

The magnetic self-energy can be expressed using the digamma function

$$\psi(z) := \frac{d}{dz} \log \Gamma(z) = \frac{\Gamma'(z)}{\Gamma(z)}. \quad (45)$$

Namely, we get

$$\int_{\mathbb{R}^2} |\mathbf{A}_{\varrho^a}|^2 \varrho^a = \vartheta(a),$$

where

$$\vartheta(a) := (2a-1)(2\psi(4a-1) - \psi(2a) - \psi(6a-2)). \quad (46)$$

This can be shown by evaluating

$$\int_{\mathbb{R}^2} |\mathbf{A}_{\varrho^a}|^2 \varrho^a = 2(2a-1) \int_0^\infty \frac{(1 - (1+r^2)^{-(2a-1)})^2}{r(1+r^2)^{2a}} dr$$

using a change of variables $t = 1 + r^2$, and the digamma function identity

$$\int_1^\infty \frac{t^{-b} - t^{-a}}{t-1} dt = \psi(b) - \psi(a), \quad (47)$$

valid for $a, b \in \mathbb{C}$ with positive real part.

We now consider the rescaled state ϕ_{λ}^a . At the optimal scale $\lambda = \lambda_*$ (see (36)), we have the total energy

$$\mathcal{E}_{\beta, \gamma, V_h} [\phi_{\lambda_*}^a] = \frac{1}{\sqrt{a-1}} \sqrt{\frac{4a(2a-1)}{(2a+1)} + \frac{1}{\pi} \frac{2a-1}{4a-1} \gamma + 2\vartheta(a)\beta^2}. \quad (48)$$

For fixed (β, γ) , this expression can be numerically optimized over $a > 1$. This has been done using Mathematica, and the resulting curve for $\gamma = 2\pi\beta\kappa$ is the thick yellow line in the plots.

We note that the Gaussian can be re-obtained by e.g. setting $a = 2/b$, $\lambda = \sqrt{b/2}$, and taking the limit $b \rightarrow 0$. Hence the state ϕ_a can (for optimal $a > 1$) be expected to have a lower energy than the Gaussian state.

We also note that along the critical line $\gamma = -2\pi\beta$, the optimal energy $\mathcal{E}_{\beta, \gamma, V_h} [\phi_{\lambda_*}^a]$ tends to 0 as β tends to the critical value $\beta = 2$. This may indeed be derived analytically using the observations

$$\psi(z+1) = \psi(z) + \frac{1}{z}, \quad \psi'(z+1) = \psi'(z) - \frac{1}{z^2},$$

which follow from the identity $\Gamma(z+1) = z\Gamma(z)$.

Vortex rings

Finally, we consider a symmetric NLL ‘‘vortex ring’’ state of degree (vorticity) $n-1 > 0$, centered at $w=0$:

$$\phi(z) = \sqrt{\frac{n}{\pi}} \frac{\bar{z}^{n-1}}{|z|^{2n} + 1}. \quad (49)$$

In polar coordinates, $z = re^{i\theta}$, we have

$$\phi(z) = \sqrt{\frac{n}{\pi}} \frac{r^{n-1} e^{-i(n-1)\theta}}{r^{2n} + 1}.$$

The corresponding density

$$\varrho(r) = \frac{n}{\pi} \frac{r^{2(n-1)}}{(r^{2n} + 1)^2}$$

is radially symmetric and normalized: $\int_{\mathbb{R}^2} \varrho = 1$. The magnetic-kinetic self-energy has already been computed in [65, Prop. 3.35 (proof)] using the supersymmetric factorization method:

$$\mathcal{E}_{\beta, \gamma = -2\pi\beta, 0} [\phi] = (\beta - 2n)^2 \frac{1}{6} \Gamma\left(1 + \frac{1}{n}\right) \Gamma\left(3 - \frac{1}{n}\right),$$

which, with the scalar self-energy

$$\int_{\mathbb{R}^2} \varrho^2 = \frac{n}{6\pi} \Gamma\left(2 - \frac{1}{n}\right) \Gamma\left(2 + \frac{1}{n}\right),$$

yields the total magnetic-kinetic self-energy:

$$K_1 = \mathcal{E}_{\beta, \gamma, 0} [\phi] = \mathcal{E}_{\beta, -2\pi\beta, 0} [\phi] + (2\pi\beta + \gamma) \int_{\mathbb{R}^2} \varrho^2.$$

The potential energy is

$$U_1 = \int_{\mathbb{R}^2} V_h \varrho = \Gamma\left(1 + \frac{1}{n}\right) \Gamma\left(1 - \frac{1}{n}\right) = \frac{\pi/n}{\sin(\pi/n)},$$

using the beta function identity

$$B(z_1, z_2) = \frac{\Gamma(z_1)\Gamma(z_2)}{\Gamma(z_1 + z_2)} = \int_0^\infty \frac{t^{z_1-1}}{(t+1)^{z_1+z_2}} dt,$$

and Euler’s reflection formula,

$$\Gamma(1+z)\Gamma(1-z) = \frac{\pi z}{\sin(\pi z)}.$$

Hence, at the optimal scaling parameter $\lambda = \lambda_*$ (see (36)), the minimal total energy becomes

$$\begin{aligned} \mathcal{E}_{\beta, \gamma, V_h} [\phi_{\lambda_*}] &= \sqrt{\frac{2}{3}} \sqrt{(\beta - 2n)^2 \left(2 - \frac{1}{n}\right) + (2\pi\beta + \gamma) \frac{n+1}{\pi}} \\ &\times \sqrt{1 - \frac{1}{n}} \frac{\pi/n}{\sin(\pi/n)}. \end{aligned}$$

For $n \in \{2, 3, 4, 5\}$ (vorticity 1, 2, 3, 4) and $\gamma = 2\pi\beta\kappa$, these are the solid purple, orange, green, respectively blue curves in the plots. Note that indeed $\mathcal{E} \rightarrow 0$ linearly as $\beta \rightarrow 2n$ and $\kappa = -1$.

Numerical data: Matlab (unconstrained)

Here we tabulate approximate energies of (2) computed in Matlab and optimized using a steepest descent algorithm adopted from [62]. As initial states we have started from the states generated in the work [62] with $\gamma = 0$, and adjusted the parameters (β, γ) to nearby values in order to generate approximate ground states with different vorticities (the number of vortices listed is approximate in non-symmetric cases). In the stable regime away from criticality, convergence to the desired precision is typically achieved after 50-200 iterations of the algorithm. Due to geometrically and topologically induced metastability, the energy converges into a local minimum, and the global minimum may only be found by comparing a set of reasonable vorticities. Some chosen initial states exhibit sufficient metastability that they can produce estimates for excited states well above the ground levels, by stopping the algorithm after a limited number of iterations during which a stable phase is shown. Thus, all numerically computed energies are only valid as approximate upper bounds to the true ground-state energy, but may also yield indications of higher resonances. At criticality $\kappa = -1$ we have only been able to obtain sufficiently stable and reliable numerics for radially symmetric states. We have also noted some observations, such as approximate linearity, comparison to analytical energies¹, or cases where we suspect that the state is far from converged. The resulting energies are shown in the plots using solid markers (colors and shapes indicate numbers of visible vortices; see legend in Fig. 4 (bottom)).

β	γ/π	#vortices	$\mathcal{E}[\phi]$	Remark
0	-1.8	0	0.789	
	-1	0	1.396	
	0	0	2.000	exact: 2
	0	1	4.000	exact: 4
	2	0	2.810	$E^{\text{TF}}(\gamma) \approx 1.886$
	3.18	0	3.184	BC: 3.1846
	15.92	0	5.793	BC: 5.7920
	20	0	6.399	$E^{\text{TF}}(\gamma) \approx 5.963$
	31.84	0	7.893	BC: 7.8918
	79.58	0	12.158	BC: 12.1578
	159.16	0	17.024	BC: 17.0236
	200	0	19.042	$E^{\text{TF}}(\gamma) \approx 18.856$
	2000	0	59.703	$E^{\text{TF}}(\gamma) \approx 59.628$
0.1	-0.2	0	1.900	linear
	-0.2	1	3.899	linear?
	0	0	2.003	
	0	1	3.950	
	0.2	0	2.100	linear
	0.2	1	4.001	
0.5	-1	0	1.500	linear
	-1	1	3.500	linear
	0	0	2.071	
	0	1	3.774	
	1	0	2.500	linear
	1	1	4.030	

TABLE I. Energies computed in Matlab. BC is comparison to Bao–Cai [16, Table 3.5] (note factor 2 and possible rounding errors).

¹ Note that the constant c was denoted by $e(1,1)/(2\pi)$ in the earlier work [62].

β	γ/π	#vortices	$\mathcal{E}[\phi]$	Remark
1	-2	0	1.003	linear?
	-2	1	3.013	linear?
-1.8	0		1.204	
-1.8	1		3.078	
0	0		2.268	$E^{\text{TF}}(2\pi c) \approx 2.050$
0	1		3.607	
1	0		2.662	
2	0		3.000	linear
2	1		4.120	
1.5	-3	0	0.631	unconverged?
	-3	1	2.542	unconverged?
0	0		2.560	
0	1		3.505	
3	0		3.500	linear
3	1		4.265	
1.9	-3.8	0	0.188	unconverged?

TABLE II. Energies computed in Matlab.

β	γ/π	#vortices	$\mathcal{E}[\phi]$	Remark
3	-6	0	1.393	
	-6	1	1.000	linear
-5.4	0		1.860	
-5.4	1		1.506	
-5	1		1.761	
0	0		3.736	
0	1		3.631	$E^{\text{TF}}(6\pi c) \approx 3.550$
6	0		5.000	linear
6	1		4.983	
3.5	-7	1	0.504	linear?

TABLE IV. Energies computed in Matlab.

β	γ/π	#vortices	$\mathcal{E}[\phi]$	Remark
2	-4	1	2.024	linear?
	-3.6	0	1.081	
-3.6	1		2.227	
-2	0		2.145	
-2	1		2.841	
0	0		2.916	$E^{\text{TF}}(4\pi c) \approx 2.899$
0	1		3.474	
2	0		3.504	
2	1		4.001	
4	0		4.000	linear
4	1		4.462	
2.5	-5	0	0.736	unconverged?
	-5	1	1.553	
0	0		3.313	
0	1		3.517	
5	0		4.500	linear
5	1		4.703	

TABLE III. Energies computed in Matlab.

β	γ/π	#vortices	$\mathcal{E}[\phi]$	Remark
4	-8	0	2.528	
	-8	1	0.090	unconverged?
-7.2	0		2.829	
-7.2	1		1.332	
-7.2	2		1.708	
-6	1		2.077	
-6	2		2.450	
-4	1		2.901	
-4	2		3.240	
-2	1		3.525	
-2	2		3.835	
0	0		4.631	
0	1		4.046	$E^{\text{TF}}(8\pi c) \approx 4.099$
0	2		4.335	
0	3		4.536	
8	0		6.000	linear
8	1		5.634	
8	2		5.878	
8	3		6.102	
16	1		6.839	
16	2		7.062	
2000	0		59.840	
2000	1		59.890	
2000	2		59.970	
4.5	-9	1	0.535	linear?

TABLE V. Energies computed in Matlab.

β	γ/π	#vortices	$\mathcal{E}[\phi]$	Remark
5	-10	0	3.546	
	-10	1	1.076	linear?
-9	1	1.850		
-9	2	1.679		
-9	3	1.805		
0	1	4.649		
0	2	4.641	$E^{\text{TF}}(10\pi c) \approx 4.583$	
0	3	4.826		
0	4	5.100		
10	1	6.377		
10	2	6.402		
10	3	6.572		
10	4	6.817		

TABLE VI. Energies computed in Matlab.

β	γ/π	#vortices	$\mathcal{E}[\phi]$	Remark
7	-13	3	1.561	
	-12.6	1	3.625	
	-12.6	2	2.127	2 or 4 vortices (ring)
	-12.6	3	1.824	
	-12.6	4	1.915	
	0	1	6.188	
	0	2	5.619	
	0	3	5.415	$E^{\text{TF}}(14\pi c) \approx 5.423$
	0	4	5.518	
	14	1	8.033	
	14	2	7.652	
	14	3	7.522	
	14	4	7.614	

TABLE VIII. Energies computed in Matlab.

β	γ/π	#vortices	$\mathcal{E}[\phi]$	Remark
6	-11.8	2	0.715	approx. ring
	-10.8	0	4.761	
	-10.8	1	2.690	
	-10.8	2	1.708	approx. ring
	-10.8	3	1.790	
	-10.8	4	2.175	
	-10	2	2.183	
	-10	3	2.246	
	-6	1	4.145	
	-6	2	3.671	
	-6	3	3.688	
	-6	4	3.959	
	0	0	6.510	
	0	1	5.379	
	0	2	5.066	$E^{\text{TF}}(12\pi c) \approx 5.021$
	0	3	5.078	
	0	4	5.314	
	12	0	8.000	linear
	12	1	7.183	
	12	2	6.992	
	12	3	7.021	
	12	4	7.220	
	2000	0	60.011	
	2000	1	59.985	
	2000	2	60.025	
	2000	3	60.081	
	2000	4	60.145	

TABLE VII. Energies computed in Matlab.

β	γ/π	#vortices	$\mathcal{E}[\phi]$	Remark
8	-15	3	1.826	3 or 6 vortices (ring)
	-15	4	1.566	
	-15	6	1.596	
	-14.4	0	6.721	
	-14.4	1	4.590	
	-14.4	3	2.145	3 or 6 vortices (ring)
	-14.4	4	1.951	$E^{\text{TF}}(1.6\pi c) \approx 1.833$
	-14.4	6	1.993	
	0	0	8.440	
	0	1	7.049	
	0	2	6.274	
	0	3	5.861	
	0	4	5.792	$E^{\text{TF}}(16\pi c) \approx 5.797$
	16	0	10.000	linear
	16	1	8.915	
	16	2	8.370	
	16	3	8.086	
	16	4	8.051	$E^{\text{TF}}(32\pi c) \approx 8.199$
	16	5	8.190	not symmetric

TABLE IX. Energies computed in Matlab.

β	γ/π	#vortices	$\mathcal{E}[\phi]$	Remark
9	-16.2	1	5.582	
	-16.2	2	3.747	2 or 4 vortices
	-16.2	6	2.216	6 or 9 vortices
	-16.2	8	2.056	4 or 8 vortices
	0	1	7.944	
	0	2	7.011	2 or 4 vortices
	0	4	6.160	$E^{\text{TF}}(18\pi c) \approx 6.149$
	0	6	6.298	
	18	1	9.819	
	18	2	9.136	
	18	4	8.544	
	18	6	8.690	

TABLE X. Energies computed in Matlab.

β	γ/π	#vortices	$\mathcal{E}[\phi]$	Remark
50	-90	40	4.721	$E^{\text{TF}}(10\pi c) \approx 4.583$
	-50	40	10.370	$E^{\text{TF}}(50\pi c) \approx 10.249$
	0	40	14.502	$E^{\text{TF}}(100\pi c) \approx 14.494$
	100	40	20.228	$E^{\text{TF}}(200\pi c) \approx 20.497$
	200	40	24.552	$E^{\text{TF}}(300\pi c) \approx 25.104$
100	-180	88	6.654	$E^{\text{TF}}(20\pi c) \approx 6.482$
	-100	88	14.643	$E^{\text{TF}}(100\pi c) \approx 14.494$
	0	88	20.499	$E^{\text{TF}}(200\pi c) \approx 20.497$
	200	87	28.612	$E^{\text{TF}}(400\pi c) \approx 28.987$
	400	88	34.748	$E^{\text{TF}}(600\pi c) \approx 35.502$

TABLE XII. Energies computed in Matlab.

β	γ/π	#vortices	$\mathcal{E}[\phi]$	Remark
10	-18	0	8.602	fast collapsing ring
	-18	1	6.588	
	-18	3	3.171	3 or 6 vortices (ring)
	-18	6	2.175	$E^{\text{TF}}(2\pi c) \approx 2.050$
	-18	8	2.263	
	-18	9	2.296	
	-10	6	4.702	
	-10	8	4.804	
	0	0	10.392	
	0	1	8.862	
	0	2	7.808	
	0	3	7.040	
	0	6	6.543	$E^{\text{TF}}(20\pi c) \approx 6.482$
	0	8	6.619	
	10	4	7.967	
	20	1	10.741	
	20	3	9.387	
	20	4	9.095	
	20	6	9.066	$E^{\text{TF}}(40\pi c) \approx 9.167$
	40	4	10.979	
	80	4	13.959	
	160	4	18.473	
	200	4	20.344	$E^{\text{TF}}(220\pi c) \approx 21.498$
	2000	4	60.277	$E^{\text{TF}}(2020\pi c) \approx 65.141$

TABLE XI. Energies computed in Matlab.

Numerical data: Mathematica (NLL constraint)

Finally, we use the above analytical solutions to the Wronskian problem for $\beta = 2n \in \{4, 6, 8\}$ to estimate the lowest energy of corresponding NLL states with relaxed radial constraints on the density (a macroscopic, averaged symmetry is still expected due to the radial potential). For $d := \deg W \in \{2, 3, 4\}$, we place the vortices in a circle of radius $R \geq 0$: $w_k = Re^{i2\pi k/d}$, while for $d = 5$ we put one at the origin and the remaining four in a circle; compare (26)–(28). Further, we choose $\eta = 0$ due to symmetry, and then numerically optimize the energy over the remaining parameters $\lambda > 0$ and $R \geq 0$. This optimization is done in Mathematica by first scanning for reasonable initial values in a rough energy plot and then iteratively rescaling the state as in (34)–(35) in order that the kinetic and potential energies eventually match (convergence towards a fixed point). At given parameter values, the energy is computed by numerical integration of the analytical density of (16) in (10) on a finite domain containing almost all of the mass. The resulting minimal energies are shown in the plots using hollow markers (colors and shapes match the previous vortex numbers; see legend in Fig. 4 (bottom)).

β	$\deg W$	γ/π	R	λ^{-1}	$\mathcal{E}[\phi_{P,Q}]$	Remark
4	1	-7.2	0	0.8944	1.4049	
	1	-6	0	1.4142	2.2214	
	1	-4	0	2.0000	3.1416	
	1	0	0	2.8284	4.4428	
	1	8	0	4.0000	6.2832	
	2	-7.2	0.6054	0.7265	2.7760	
	2	-6	0.6860	1.0290	4.4693	
	2	-4	0.8774	1.1965	5.8111	
	2	0	1.1519	1.3823	7.6549	
	2	8	1.5034	1.6108	10.3610	
6	2	-10.8	0	1.8724	1.7661	
	2	-6	0	6.2614	3.9487	
	2	0	0	10.5320	5.5838	
	2	12	0	17.7194	7.8948	
	3	-10.8	0.5055	2.0858	2.3043	
	3	-6	0.8344	3.9167	4.5982	
	3	0	0.9697	5.6420	6.4626	
	3	12	1.1428	8.0949	9.1033	
	4	-10.8	0.8861	0.9747	3.7769	errors
	4	-6	1.3621	1.5437	7.8009	
	4	0	1.53552	2.1498	10.8994	
	4	12	1.9367	2.4209	14.3487	

TABLE XIII. Energies for optimized NLL states.

β	$\deg W$	γ/π	R	λ^{-1}	$\mathcal{E}[\phi_{P,Q}]$	Remark
8	3	-14.4	0	4.0000	2.2214	errors
	3	-14	0	5.0000	2.4360	
	3	-8	0	20.0010	4.9673	
	3	0	0	40.0021	7.0247	
	3	8	0	60.0031	8.6034	
	3	16	0	80.0042	9.9334	
	4	-14.4	0.5859	3.4455	2.1411	(a)
	4	-14	0.6235	4.0390	2.3895	(b)
	4	-8	0.8845	11.3902	4.7762	(c)
	4	0	1.0640	19.0020	6.7574	(d)
	4	8	1.1502	26.4183	8.2982	
	4	16	1.2622	32.0333	9.5480	
	5	-14.4	0.9204	2.5415	2.6768	
	5	-14	0.8534	2.9129	2.7407	
	5	-8	1.17602	5.9547	5.4152	errors
	5	0	1.4431	8.3299	7.6605	
	5	8	1.5369	10.4986	9.2824	
	5	16	1.6036	12.5713	10.7563	

TABLE XIV. Energies for optimized NLL states.

Remarks:

Some of the numerical integrations reported errors regardless of precision and may therefore be less reliable.

(a) The energy at the lowest radial vortex ring here ($n = 4$) is $\pi/\sqrt{2} \approx 2.2214$.

(b) The energy at the lowest radial vortex ring here ($n = 4$) is $\sqrt{5/2}\pi/2 \approx 2.4836$.

(c) The energy at the lowest radial vortex ring here ($n = 4$) is $\sqrt{5/2}\pi \approx 4.9673$.

(d) The energy at the lowest radial vortex ring here ($n = 3$) is $8\sqrt{53}\pi/27 \approx 6.7766$.